POLITECNICO DI TORINO
Repository ISTITUZIONALE

Advancing Mistuning Identification and Dynamic Modeling of Blisks Through Blade Detuning Tests

Original
Advancing Mistuning Identification and Dynamic Modeling of Blisks Through Blade Detuning Tests / Zhou, Biao; Li, Ankang; Battiato, Giuseppe; Berruti, Teresa M.. - In: JOURNAL OF PROPULSION AND POWER. - ISSN 0748-4658. - (2024), pp. -12. [10.2514/1.b39365]

Availability:
This version is available at: 11583/2986203 since: 2024-02-21T14:09:52Z

Publisher:
American Institute of Aeronautics and Astronautics

Published
DOI:10.2514/1.b39365

Terms of use:

This article is made available under terms and conditions as specified in the corresponding bibliographic description in the repository

Publisher copyright
AIAA preprint/submitted version e/o postprint/Author's Accepted Manuscript

(Article begins on next page)

28 April 2024

below, substantially differs from the identification procedure proposed in [14].

Step 1: Quantification of residual inter-blade coupling.

This step aims to numerically estimate the *a-priori* unknown influence coefficients in $\boldsymbol{\psi}$, rather than to exactly reproduce the realistic blade detuning test results. To this end, the experimentally determined blade modulus mistuning pattern $\boldsymbol{\delta}^{\mathrm{V}} = {}^{E}\boldsymbol{\delta}_m^{\mathrm{bdt}}$ into a tuned blisk FEM with detuning mass, and then the blade-by-blade impact tests are simulated. The superscript $(.)^{\mathrm{V}}$ reads as virtual test by numerical simulation. Similar to the preceding realistic blade detuning tests, the virtual test yields an isolated peak frequency $\omega_{m,j}^{\mathrm{V}}$ for the m-th mode of the blade j. At this point, Eq. 8 for all the N blades in the virtual tests are collected and reshaped as:

$$\begin{bmatrix} \frac{(\omega_{m,1}^{\mathrm{V}})^2-\omega_{\mathrm{ref}}^2}{\omega_{\mathrm{ref}}^2} \\ \frac{(\omega_{m,2}^{\mathrm{V}})^2-\omega_{\mathrm{ref}}^2}{\omega_{\mathrm{ref}}^2} \\ \vdots \\ \frac{(\omega_{m,N}^{\mathrm{V}})^2-\omega_{\mathrm{ref}}^2}{\omega_{\mathrm{ref}}^2} \end{bmatrix} = \begin{bmatrix} \delta_1^{\mathrm{V}} & \delta_2^{\mathrm{V}} & \cdots & \delta_N^{\mathrm{V}} \\ \delta_2^{\mathrm{V}} & \delta_3^{\mathrm{V}} & \cdots & \delta_1^{\mathrm{V}} \\ \vdots & \ddots & \ddots & \vdots \\ \delta_N^{\mathrm{V}} & \delta_1^{\mathrm{V}} & \cdots & \delta_{N-1}^{\mathrm{V}} \end{bmatrix} \begin{bmatrix} \psi_0 \\ \psi_1 \\ \vdots \\ \psi_{-1} \end{bmatrix} = \boldsymbol{\Delta} \cdot \boldsymbol{\psi}({}^{E}\boldsymbol{\delta}_m^{\mathrm{bdt}}) \tag{9}$$

where $\boldsymbol{\Delta}$ is a circulant matrix that is composed of the prescribed blade modulus mistuning values δ_i^{V} with $i = 1, 2, \ldots N$.

The influence coefficients in $\boldsymbol{\psi}({}^{E}\boldsymbol{\delta}_m^{\mathrm{bdt}})$ can be obtained by solving Eq. 9. Moreover, $\boldsymbol{\psi}({}^{E}\boldsymbol{\delta}_m^{\mathrm{bdt}})$ is considered as a close approximation of $\boldsymbol{\psi}({}^{E}_{\mathrm{ref}}\boldsymbol{\delta}_m)$ in the sense that the experimentally determined blade mistuning pattern ${}^{E}\boldsymbol{\delta}_m^{\mathrm{bdt}}$ in the realistic blade detuning tests is a fair approximation of the 'true' blade modulus mistuning pattern ${}^{E}_{\mathrm{ref}}\boldsymbol{\delta}_m$.

Step 2: Inclusion of residual inter-blade coupling for mistuning identification.

The second step is to identify the 'true' blade modulus mistuning pattern ${}^{E}_{\mathrm{ref}}\boldsymbol{\delta}_m$ by Eq. 8. The residual inter-blade coupling within the real blisk test piece is included by assuming $\boldsymbol{\psi}({}^{E}_{\mathrm{ref}}\boldsymbol{\delta}_m) \approx \boldsymbol{\psi}({}^{E}\boldsymbol{\delta}_m^{\mathrm{bdt}})$. Recall Eq. 8 for all the N blades in the realistic blade detuning tests and rewrite them as:

$$\begin{bmatrix} \frac{(\omega_{m,1}^{\mathrm{bdt}})^2-\omega_{\mathrm{ref}}^2}{\omega_{\mathrm{ref}}^2} \\ \frac{(\omega_{m,2}^{\mathrm{bdt}})^2-\omega_{\mathrm{ref}}^2}{\omega_{\mathrm{ref}}^2} \\ \vdots \\ \frac{(\omega_{m,N}^{\mathrm{bdt}})^2-\omega_{\mathrm{ref}}^2}{\omega_{\mathrm{ref}}^2} \end{bmatrix} = \begin{bmatrix} \psi_0 & \psi_1 & \cdots & \psi_{-1} \\ \psi_{-1} & \psi_0 & \cdots & \psi_{-2} \\ \vdots & \ddots & \ddots & \vdots \\ \psi_1 & \cdots & \psi_{-1} & \psi_0 \end{bmatrix} \begin{bmatrix} {}^{E}_{\mathrm{ref}}\delta_{m,1} \\ {}^{E}_{\mathrm{ref}}\delta_{m,2} \\ \vdots \\ {}^{E}_{\mathrm{ref}}\delta_{m,N} \end{bmatrix} = \boldsymbol{\Psi} \cdot {}^{E}_{\mathrm{ref}}\boldsymbol{\delta}_m \tag{10}$$

where $\boldsymbol{\Psi}$ is a circulant matrix that is composed of the influence coefficients in $\boldsymbol{\psi}({}^{E}\boldsymbol{\delta}_m^{\mathrm{bdt}})$, already available after Step 1.

${}^{E}_{\mathrm{ref}}\boldsymbol{\delta}_m$, which is also referenced to ω_{ref} previously prescribed in Eq. 9 can be readily identified by solving Eq. (10). In practice, the identified blade modulus mistuning pattern is transformed into ${}^{E}\boldsymbol{\delta}_m^{\mathrm{BDTID}}$ or the equivalent frequency mistuning pattern ${}^{f}\boldsymbol{\delta}_m^{\mathrm{BDTID}}$ with a zero mean.

For Peer Review

The identification results by BDTID are graphically presented in Fig. 7. The mode-depend blade decoupling performance in Fig. 6 can be well explained by observing the influence coefficients for the target 1B and 1T blade mode, respectively. Note that $\psi_0 = 0.462$ for 1B mode in Fig. 7a indicates that there remains a high level of residual inter-blade coupling during the blade detuning tests and that the experimentally determined blade mistuning pattern ${}^f\boldsymbol{\delta}_{1B}^{bdt}$ is not accurate enough. The correction procedure compensates for the inadequate mass detuning effect, and gives the identified blade mistuning pattern ${}^f\boldsymbol{\delta}_{1B}^{BDTID}$ quite different from ${}^f\boldsymbol{\delta}_{1B}^{bdt}$ in Fig. 7c. On the contrary, Fig. 7b reveals that the residual inter-blade coupling is negligible for the 1T mode with $\psi_0 = 0.944$ close to 1. This implies that the blade detuning tests already give a fairly good estimation of the 'true' mistuning pattern by ${}^f\boldsymbol{\delta}_{1T}^{bdt}$. Improvement of ${}^f\boldsymbol{\delta}_{1T}^{BDTID}$ by the correction procedure is thus barely visible in Fig. 7d.

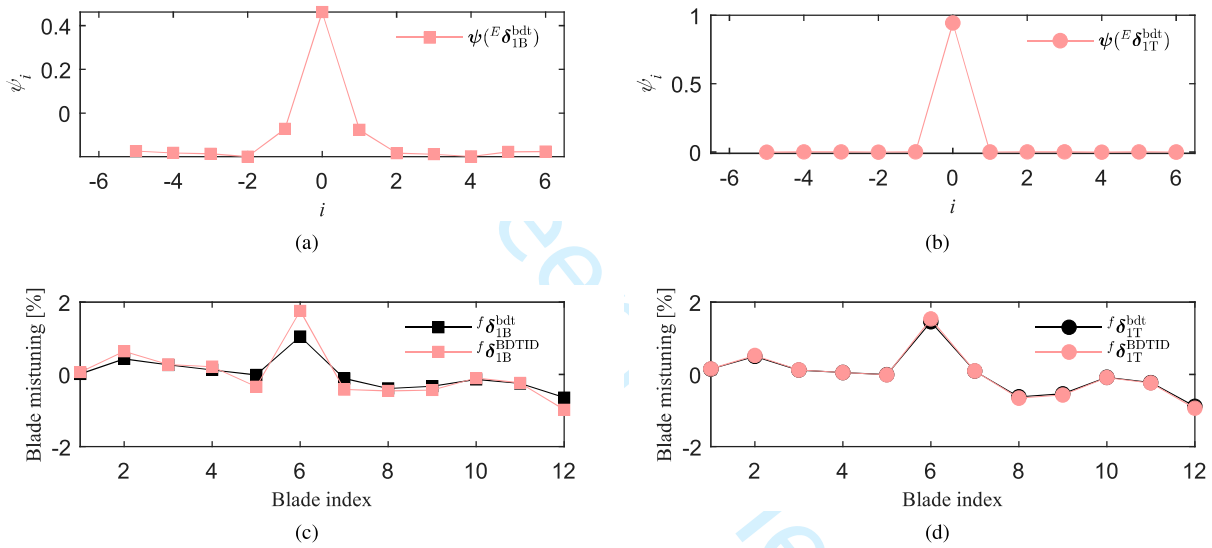

Fig. 7 Identification results by BDTID: (a) influence coefficients for 1B mode; (b) influence coefficients for 1T mode; (c) 1B blade mistuning pattern; (d) 1T blade mistuning pattern.

The mode-dependent blade detuning tests and mistuning identification results are attributed to the different inter-blade coupling strength of the blisk mode families, since the quantity and position of blade detuning mass is fixed during the test. Compared with the 1B mode family, the 1T mode family, having a favorable lower inter-blade coupling strength (see Fig. 2), is better decoupled into a single blade mode by the detuning masses.

2. Robustness of BDTID

Robustness of the BDTID method with respect to different blade detuning test quality is hereafter examined. Similar with the preceding test setup in Fig. 5a, blade detuning tests are carried out with 4 squared magnets (a total weight of $4m^d = 7$g, see Fig. 8a) and 8 squared magnets (a total weight of $8m^d = 14$g, see Fig. 8b) on each blade, respectively. Position of the multiple magnets is basically consistent to cover the blade surface area with high kinetic energy density

Review copy- Do not distribute

for both 1B and 1T blade modes.

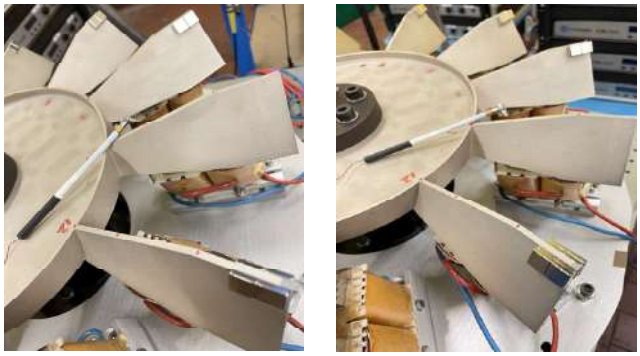

(a) (b)

Fig. 8 Blade detuning tests with: (a) 4 squared detuninng masses; (b) 8 squared detuninng masses.

In order to portray the impact of the varying detuning mass on the blade detuning test quality, the experimentally acquired FRFs at blade 1 are collected and compared in Fig. 9. For instance, the FRF derived in the blade detuning test with 2 squared magnets is denoted as 'BDT-2S', and so forth. In the frequency range of the 1B mode family, a general frequency shift to the left can be observed for the BDT FRFs with increasing detuning mass in Fig. 9a. Meanwhile, the minor peaks gradually fade out of the frequency range of interest. This signifies that the increasing detuning mass quantity gives an improved blade mode decoupling performance for the 1B mode. However, it is not the case for the 1T mode in Fig. 9b. In spite of the increasing detuning mass, the single peak arising in the individual BDT FRFs around 1T mode family nearly overlap with each other, giving always a good blade mode decoupling performance.

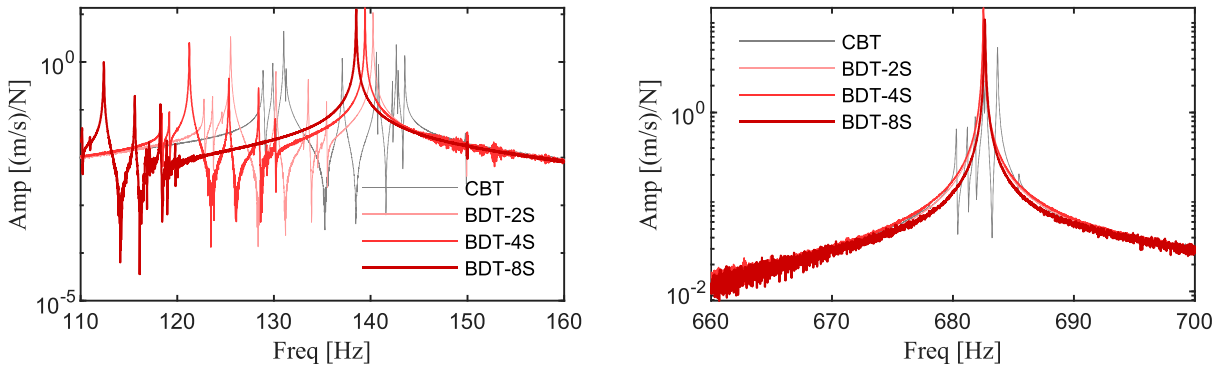

Fig. 9 FRFs at blade 1 in blade detuning tests with different detuning masses: (a) around 1B mode family; (b) around 1T mode family.

The experimental evidence above is in excellent agreement with identification results by BDTID presented in Fig. 10. It can be seen in Fig. 10a that ψ_0 , as an indicator of the residual inter-blade coupling and blade mode isolation for

Review copy- Do not distribute

1B mode, escalates from 0.462 (BDT-2S) to 0.652 (BDT-4S) and to 0.705 (BDT-8S). This quantitative measurement validates the experimental observation in Fig. 9a. Due to the strong inherent inter-blade coupling of the 1B mode family, the increasing detuning mass does not necessarily lead to a perfect vibration isolation for 1B blade mode since the value of ψ_0 is still far below 1. Nevertheless, Fig. 10c shows that, after the correction procedure, a satisfactory consistency is achieved among the identified 1B blade mistuning patterns in the three cases. This highlights the robustness of proposed correction procedure. It succeeds to capture the inherent blade mistuning even in the event of less adequate mass detuning effect, e.g. in the BDT-2S case. By comparison, it can be observed that the influence coefficients for 1T mode (see Fig. 10b) and the identified 1T blade mistuning patterns (see Fig. 10d) are insensitive to the variation of the detuning mass. Once again, the reason is that the relatively weak inter-blade coupling of the 1T mode family already leads to a good blade mode isolation during the blade detuning tests.

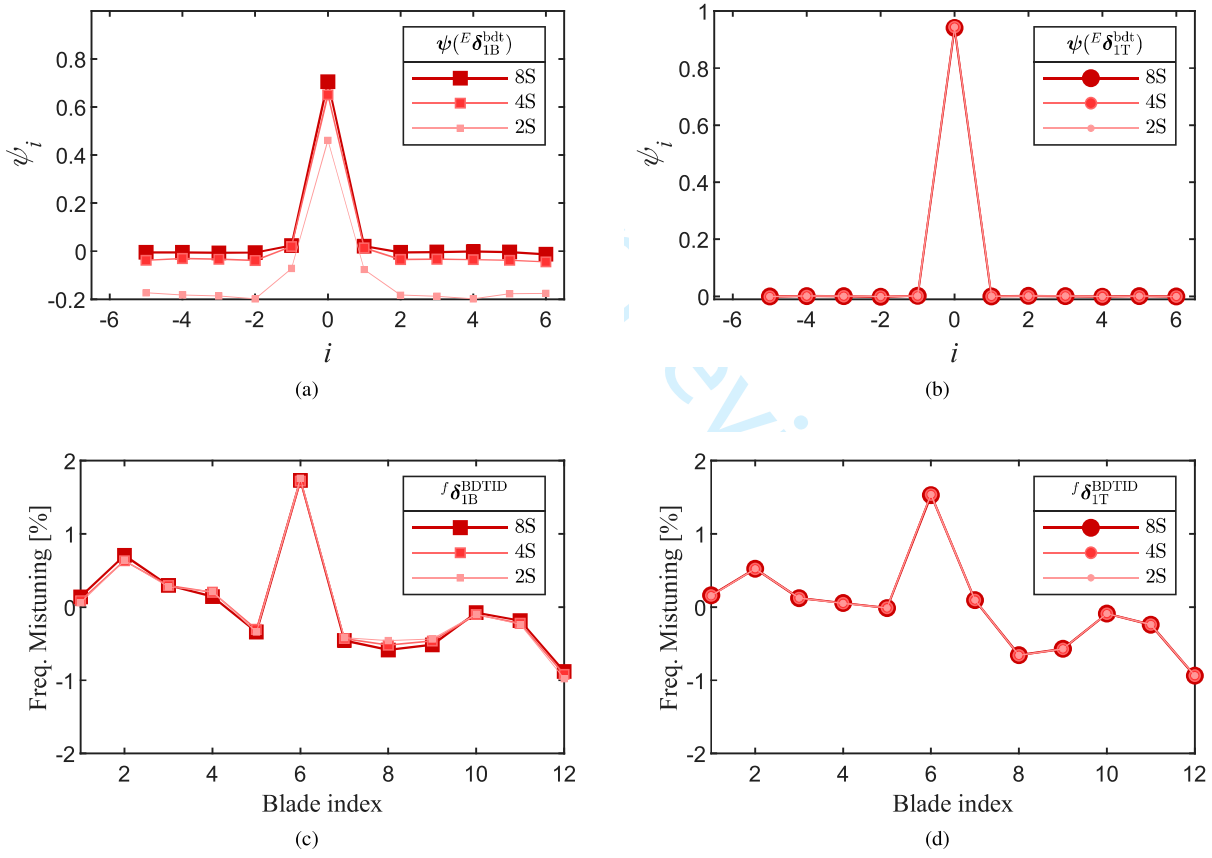

Fig. 10 BDTID results with different detuning mass: (a) influence coefficients for 1B mode; (b) influence coefficients for 1T mode; (c) 1B blade mistuning pattern; (d) 1T blade mistuning pattern.

In sum, blade detuning test quality is governed by a number of factors, including the inherent inter-blade coupling strength of the blisk mode family, the position and quantity/magnitude of the detuning masses. A fundamental function

Review copy- Do not distribute

of the proposed correction procedure, is to quantitatively evaluate the blade detuning test quality by the value of influence coefficient ψ_0. Most importantly, by compensating for the residual inter-blade coupling, this correction procedure is capable of retrieving the 'true' blade mistuning even when the blade detuning test quality is not so good.

3. Model-BDTID

From here on, for the sake of conciseness, only the representative blade mistuning patterns identified from the blade detuning tests with 8 squared magnets as detuning mass (BDT-8S) are presented. The Model-BDTID is constructed by injecting the blade modulus mistuning patterns ${}^{E}\boldsymbol{\delta}_m^{\mathrm{BDTID}}$ into a tuned blisk FEM. Note that the tuned blisk FEM is *a-priori* calibrated to account for the non-ideal boundary condition. This is realized by respectivly adjusting the Young's modulus values of the blades and disk part within the blisk such that its natural frequency of the 1B mode family at ND0 (which is barely affected by blade mistuning) matches the corresponding peak frequency clearly identifiable in the CBT FRF. The resultant mistuned blisk model (Model-BDTID) should then represent the real blisk with high accuracy.

III. Model Verification for the Mistuned Blisk

The different dynamic models of the blisk previously presented will be verified against the experimental data extracted from the modal test (i.e. measured natural frequencies and one-point-per-blade mode shapes). Their performance in predicting the modal behaviours of the blisk test piece will be evaluated.

A. Model-FMMID

Model-FMMID of the blisk takes the form of a FMM reduced-order model. It enables to calculate the mistuned system frequencies and modes at negligible computational cost. Modal correlation by the Modal Assurance Criterion Analysis (MAC) is carried out to quantify the discrepancy between the experimental reference data and the model-reconstructed data sets, as presented in Fig. 11.

Clearly, correlation between the experimental/numerically reconstructed full-blisk modes of 1B family is not close enough since the MAC matrix in Fig. 11a shows a certain number of off-diagonal terms. By contrast, a very good match is achieved in Fig. 11b for both the mistuned blisk frequencies and mode shapes of the 1T mode family, indicating that the identified 1T blade mistuning is of high accuracy. Notice that the 1B mode family is characterized by stronger inter-blade coupling, and accordingly by more disk participation in the modal vibration, than the 1T mode family (see Fig. 2). It is thus inferred that the high disk participation is responsible for inadequate accuracy of the identified 1B blade mistuning. It is well known that FMMID requires that the target blisk mode family should have the modal strain energy primarily in the blades, e.g. the 1T mode family in the current case. However, as for the 1B mode family, FMMID identifies the blade mistuning with less accuracy, depending on the extent to which the ideal condition for FMMID is violated.

Review copy- Do not distribute

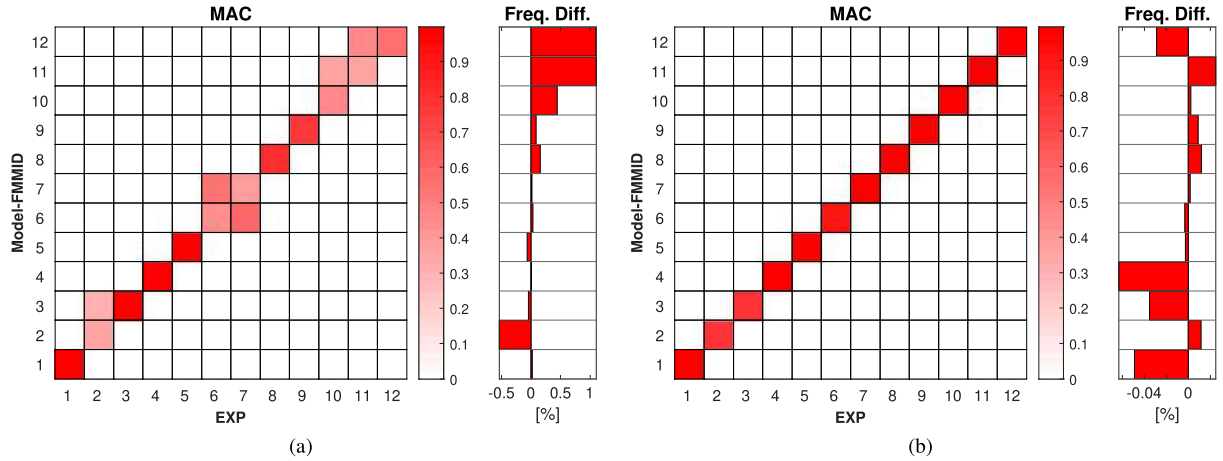

Fig. 11 Modal correlation between experimental reference data and numerically reconstructed data by Model-FMMID: (a) 1B mode family; (b) 1T mode family.

B. Model-CMMID

Similarly, Model-CMMID is a CMM reduced-order model, which allows to compute the mistuned system dynamics in an efficient way. Modal correlation is implemented between the experimental derived/ numerically reconstructed modal datasets by Model-CMMID. An improved mode correlation for 1B mode family is observed in Fig. 12a, where there are less off-diagonal terms in the MAC plot, compared with Fig. 11a. Once again, excellent modal correlation is achieved for 1T mode family in Fig. 12b. Although derived in a different form, CMMID shares a common prerequisite as FMMID that the mistuned blisk modes are closely spaced in a narrow frequency range with blade-dominant motion. Similar to the previous findings, the distinguishing modal correlation results are also attributed to the level of disk participation in the target mode family.

C. Model-BDTID

Model-BDTID is a full-order blisk model with an assigned blade modulus mistuning pattern obtained by BDTID. In order to avoid the computationally expensive full blisk simulation, the CMM ROM techniques well suited for blisks with small stiffness mistuning is adopted to compute the mistuned blisk dynamics. Fig. 13 shows that for the majority of blade-dominant modes of both 1B and 1T family, the numerical blisk modal properties reconstructed by Model-BDTID generally show high correlations with the experimental counterparts. As for the first 1 ~ 4 modes of 1B family with low frequencies in Fig. 13a, the modal discrepancies are due to uncertainties arising from the clamping boundary conditions in the disk center. Note that these 4 modes correspond to the split modes of the tuned blisk at ND1~2, which actually tend to behave as disk-dominant modes (see Fig. 2). Accordingly, the relatively high disk contribution makes them heavily affected by the disk clamping uncertainties.

In spite of the disparity for the first 4 blisk modes with relatively high disk participation, it is proved that blade

Review copy- Do not distribute

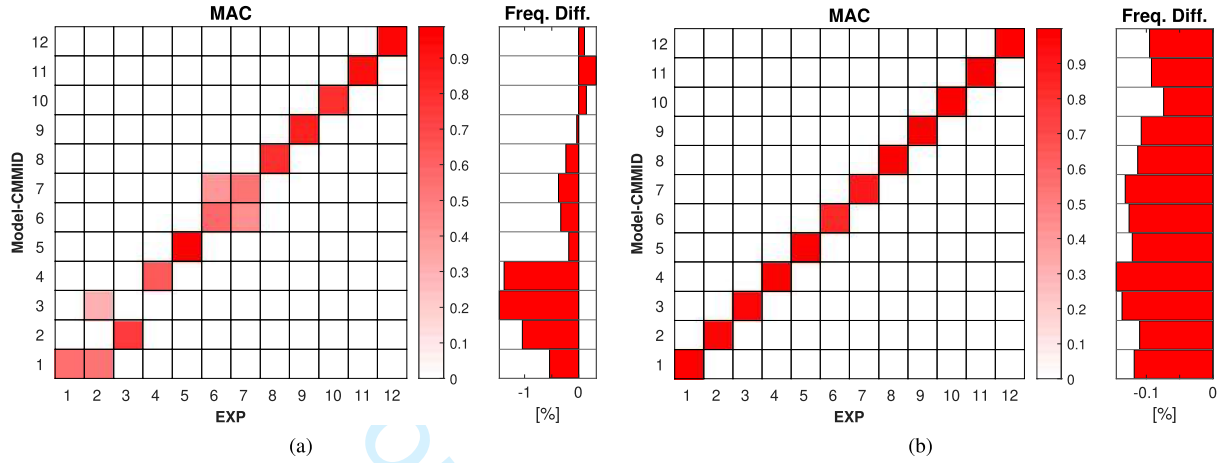

Fig. 12 Modal correlation between experimental reference data and numerically reconstructed data by Model-CMMID: (a) 1B mode family; (b) 1T mode family.

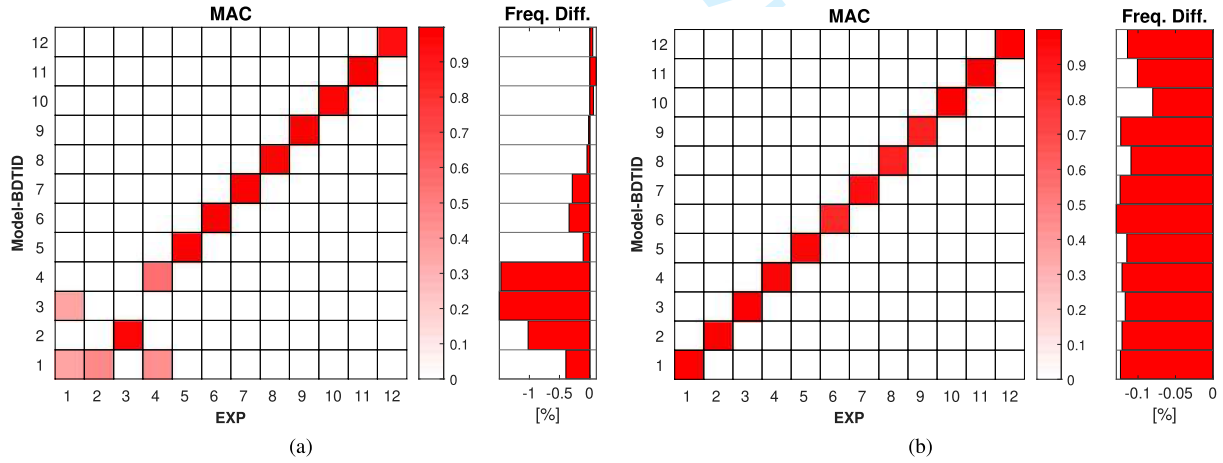

Fig. 13 Modal correlation between experimental reference data and numerically reconstructed data by Model-BDTID: (a) 1B mode family; (b) 1T mode family.

For Peer Review

mistuning of both 1B and 1T modes are identified with fairly good accuracy. The resultant Model-BDTID exhibits high accuracy in reproducing the mistuned frequencies and mode shapes of the blisk.

D. Summary

A complete collection of the experimentally identified blade frequency mistuning patterns are depicted in Fig. 14. In order to facilitate the like-for-like comparison, it is reasonable to take the blade mistuning pattern derived by BDTID as a reference. The Pearson correlation coefficient R is then computed to quantify the consistency between a certain mistuning pattern with respect to the reference. Its value is expected to be greater than 0. Values of R close to 1 denote high consistency.

Overall, there are basically good consistency (R = 0.91 by FMMID and R = 0.93 by CMMID) for the 1B blade mistuning patterns in Fig. 14a. While Fig. 14b shows close-to-perfect consistency among the 1T blade mistuning patterns. Considering the preceding model verification results, it is obvious that all the three methods give accurate blade mistuning identification results for 1T mode family with weak inter-blade coupling. It is further inferred that more disk participation in 1B mode family makes FMMID/CMMID sensitive to modal input errors. By comparison, BDTID is advantageous in this case, since it is able to capture the underlying blade mistuning with superior accuracy.

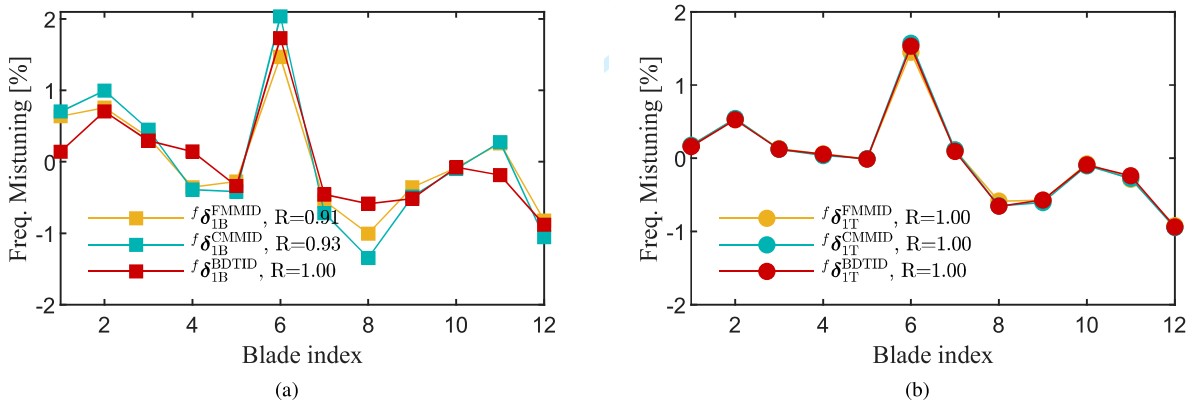

Fig. 14 Comparison of identified blade frequency mistuning patterns: (a) 1B mode; (b) 1T mode.

IV. Forced Response Tests & Model Validation

The vibration response of a blisk under traveling wave excitation typically occurring in the aero-engine is generally of great interest in practice. The point is: can the described mistuned blisk models predict the traveling wave response of the blisk with an acceptable degree of accuracy? In this section, the blisk undergoes forced response tests in a well-developed stationary traveling wave excitation test rig [22], which has already been shown in Fig. 1a. The traveling wave excitation system consists of N cyclically repeated electromagnetic (EM) units to produce the Engine Order-like

Review copy- Do not distribute

(EO) excitation. Each EM unit under individual blades is fed by a harmonic input voltage with controlled frequency, amplitude and inter-blade phase shift driven by the EO, to exert a non-contact force onto the target blade, as shown in Fig. 1c. As a prerequisite, this system requires a subtle calibration step to ensure a uniform excitation force amplitude by each EM as much as possible [23].

With a upper frequency limit of 600 Hz, this test rig allows to perform forced response tests in the frequency range covering the 1B mode family. This paper presents the forced response tests under a representative EO0 and EO3 excitation, respectively. Forced responses at the target resonant frequencies are measured at the tip of each blade in the axial direction. They are further used to validate the predictive performance of different mistuned blisk models, respectively.

A. Forced response to an EO0 excitation

Forced response amplitudes of the blisk under an EO0 excitation are measured at the resonant frequency by LDV, and collected as the Operational Deflection Shape (ODS) shown in Fig. 15a. The EO0 excitation imposes the same force amplitude on each blade without inter-blade phase shift. The measured fluctuation of blade vibration amplitudes is in consequence of blade mistuning. Fig. 15b exemplifies the forced response at blade 1 computed by the Model-FMMID. As expected, the principal resonance peak signifies that a dominant ND0 mode component is strongly excited. Comparison

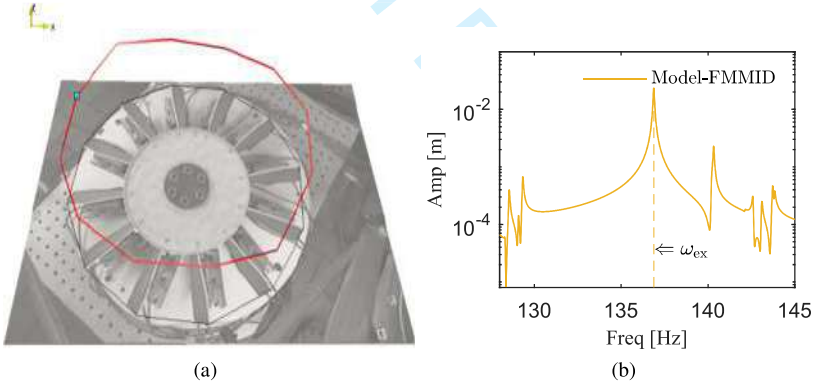

Fig. 15 Forced response to an EO0 excitation: (a) Measured ODS at the resonant frequency; (b) forced response curve at blade 1 predicted by Model-FMMID.

of the tested ODS and its numerical counterpart predicted by Model-FMMID is plotted in Fig. 16a. Since the excitation force amplitude is not available, the ODS is normalized for comparison so that the maximum blade amplitude is equal to 1. A value of MAC = 0.994 indicates a high correlation between the tested/Model-FMMID predicted ODS. Similarly, the other mistuned blisk models also predict the relative blade amplitudes with high accuracy, as shown in Fig. 16.

Review copy- Do not distribute

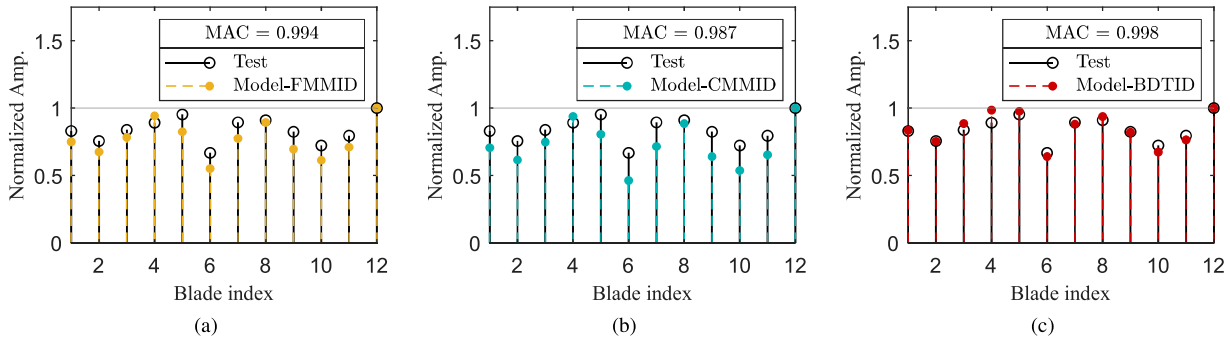

Fig. 16 Comparison of tested/model predicted ODS under an EO0 excitation: (a) Model-FMMID; (b) Model-CMMID; (c) Model-BDTID.

B. Forced response to an EO3 excitation

When it comes to the EO3 excitation, things become different. Due to blade mistuning, the tuned blisk mode pair at ND3 is split into 2 closely spaced mistuned blisk modes. They are fully excited by the EO3 excitation, giving rise to 2 tested ODS measured respectively at the corresponding peak frequency in Fig. 17. These ODS exhibit a modulated spatial wave shape, a hint of moderate mode localization due to mistuning [23].

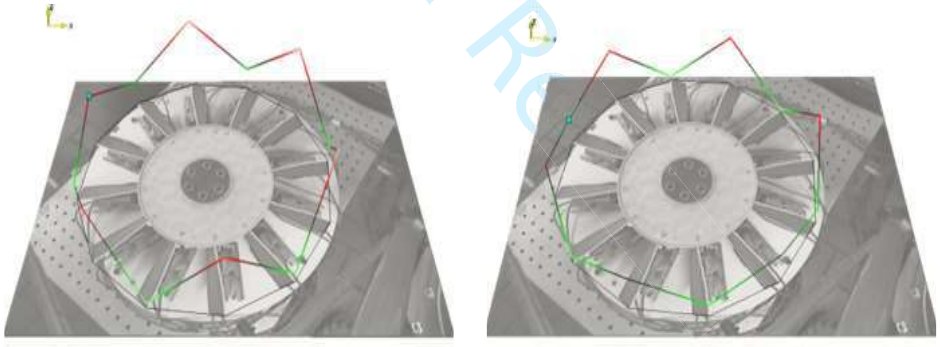

Fig. 17 Tested ODS under an EO3 excitation: (a) at $\omega_{ex,1}$; (b) At $\omega_{ex,2}$.

A complete comparison of the tested ODS under the EO3 excitation against numerical predictions is given in Fig. 18. Each row of subplots corresponds to a specific mistuned blisk model. For instance, Fig. 18a depicts the forced response curve at blade 1 computed by Model-FMMID. It enables to conduct the ODS correlation analysis at the peak frequency $\omega_{ex,1}$ (Fig. 18b) and $\omega_{ex,2}$ (Fig. 18c), respectively.

In general, poor correlations occur between the tested ODS and the numerical counterparts by Model-FMMID and Model-CMMID, as indicated by the low MAC values below 0.726. A close examination of the forced response curves further reveals that the forced response test & model validation results are in line with the preceding modal correlation

Review copy- Do not distribute

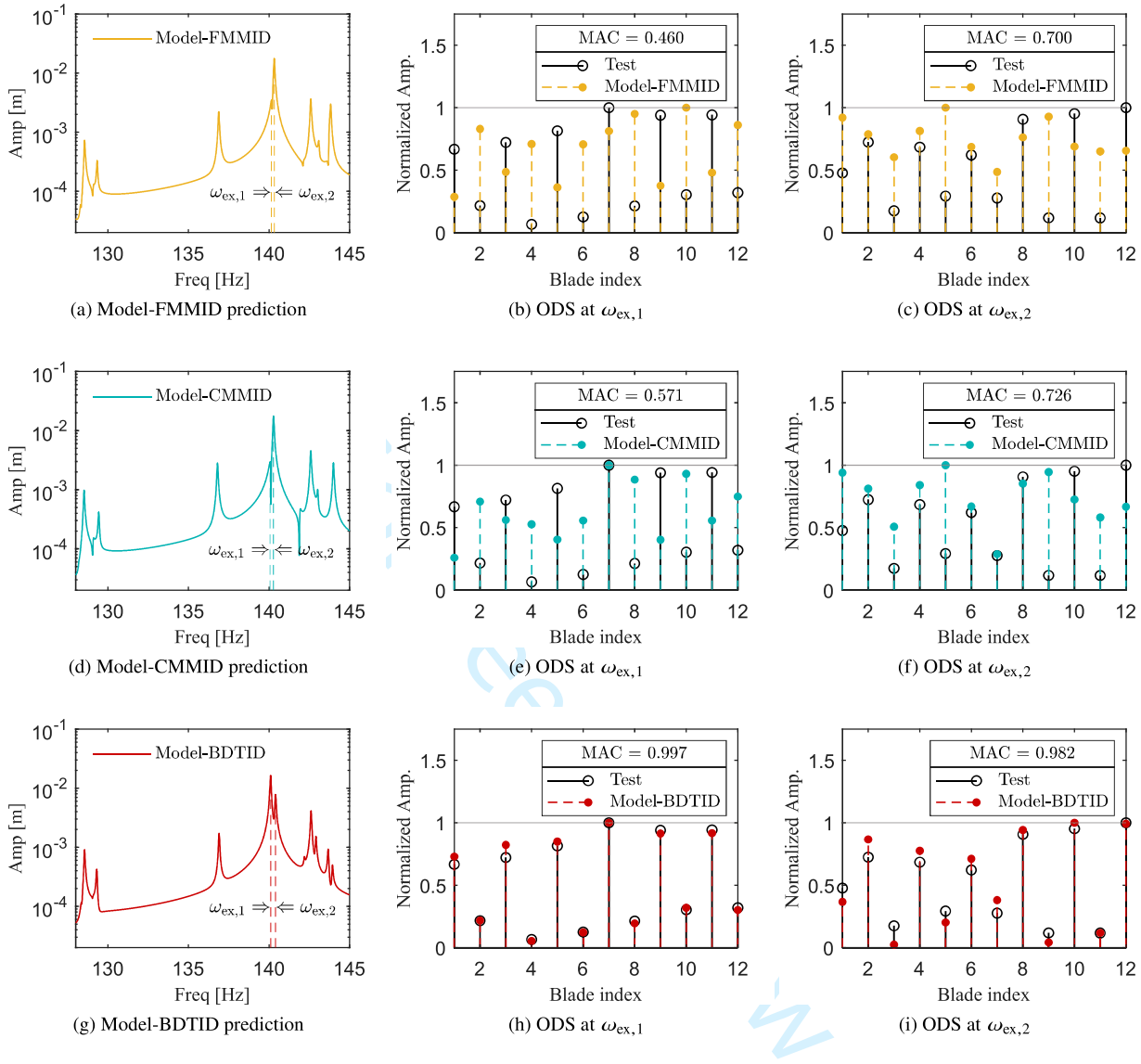

Fig. 18 Comparison of tested/model predicted ODS under an EO3 excitation.

results in Sec. III. More specifically, it can be found in the MAC plot of both Fig. 11a and Fig. 12a that there exists a mismatch between the experimentally/numerically derived modes with the index of 6 and 7, which happen to match the EO3 excitation. Apparently, insufficient accuracy of the 1B blade mistuning pattern identified by FMMID and CMMID is the most likely reason for the spurious forced response prediction.

On the contrary, the model-BDTID gives a very good prediction performance with MAC values up to 0.997 and 0.982. Hence, the previous observation about the high confidence of Model-BDTID is hereby consolidated.

V. Conclusion

In this paper, intensive test campaigns and numerical analyses were conducted for the blade mistuning identification and predictive dynamic modeling of a simplified blisk test piece. A complete assessment of the different mistuned blisk models was realized by the forced response tests and correlation analysis for the subject blisk in a stationary traveling wave excitation rig. In particular, emphasis is put on the emerging blade mistuning identification method based on blade detuning tests.

The frequency-mistuning modeling approach of blisks relies on the experimental identification of the blade mistuning in the form of blade-alone frequency/ modulus variations. Exploiting suitable reduced-oder modeling techniques, the conventional FMMID and CMMID are numerically efficient in finding a mistuning pattern that gives the best fit to the input measured blisk modes. A high-quality experimental modal analysis is thus crucial to ensure adequate accuracy of FMMID and CMMID procedures. However, this usually requires considerable expertise and intensive experimental effort. It is also found that a relatively high disk contribution in the 1B mode family is responsible for inadequate accuracy of the identified blade mistuning. Due to the high sensitivity of the blisk's response to blade mistuning, it might further lead to an inaccurate forced response prediction under engine order excitation.

On the contrary, the BDTID method consists of blade-by-blade detuning tests followed by a correction procedure. The detuning tests enable to approximately evaluate the 'blade-alone' frequencies in a direct way. The core of the correction procedure is the quantification of the residual inter-blade coupling due to mass detuning effect and its compensation in the identification of blade mistuning. It also enables to quantitatively evaluate the detuning test quality by observing the influence coefficient ψ_0. Effectiveness and robustness of BDTID has been fully demonstrated in the sense that it is able to capture the 'true' blade mistuning even in case of poor blade detuning test quality. The resultant mistuned blisk model exhibits high accuracy in the modal correlation and forced response validation results. The relatively low experimental effort requirement and proved robust performance put the BDTID at an advantage over the conventional FMMID and CMMID methods. BDTID is therefore recommended for a wide variety of scenarios in the identification practice for the purpose of predictive dynamic modeling of blisks.

For Peer Review

Funding Sources

This work has received funding from the European Union's Horizon 2020 research and innovation program under the Marie Sklodowska-Curie grant agreement No. 891197. This work is also part of a project that has received funding from National Natural Science Foundation of China (Grant No. 52175098). This support is also gratefully acknowledged.

References

[1] Salas, M. G., Bladh, R., Mårtensson, H., Petrie-Repar, P., Fransson, T., and Vogt, D. M., "Forced Response Analysis of a Mistuned, Compressor Blisk Comparing Three Different Reduced Order Model Approaches," *Journal of Engineering for Gas*

Turbines and Power, Vol. 139, No. 6, 2017. https://doi.org/10.1115/1.4035209.

[2] Tacher, A., Thouverez, F., and Armand, J., "Modelling and analysis of a bladed drum subject to the Coriolis and mistuning effects," *International Journal of Mechanical Sciences*, Vol. 215, 2022, p. 106994. https://doi.org/10.1016/j.ijmecsci.2021.106994.

[3] Feiner, D. M., and Griffin, J. H., "Mistuning identification of bladed disks using a fundamental mistuning model - Part II: Application," *Journal of Turbomachinery*, Vol. 126, No. 1, 2004, pp. 159–165. https://doi.org/10.1115/1.1643914.

[4] Madden, A. C., Castanier, M. P., and Epureanu, B. I., "Reduced-order model construction procedure for robust mistuning identification of blisks," *AIAA journal*, Vol. 40, No. 11, 2008, pp. 2890–2898. https://doi.org/10.2514/1.37314.

[5] Nyssen, F., and Golinval, J. C., "Identification of mistuning and model updating of an academic blisk based on geometry and vibration measurements," *Mechanical Systems and Signal Processing*, Vol. 68–69, 2016, pp. 252–264. https://doi.org/10.1016/j.ymssp.2015.08.006.

[6] Pichot, F., Laxalde, D., Sinou, J. J., Thouverez, F., and Lombard, J. P., "Mistuning identification for industrial blisks based on the best achievable eigenvector," *Computers and Structures*, Vol. 84, 2006, pp. 2033–2049. https://doi.org/10.1016/j.compstruc.2006.08.022.

[7] Judge, J. A., Pierre, C., and Ceccio, S. L., "Experimental mistuning identification in bladed disks using a component-mode-based reduced-order model," *AIAA journal*, Vol. 47, No. 5, 2009, pp. 1277–1287. https://doi.org/10.2514/1.41214.

[8] Chan, Y. J., and Ewins, D. J., "Prediction of Vibration Response Levels of Mistuned Integral Bladed Disks (Blisks): Robustness Studies," *Journal of Turbomachinery*, Vol. 134, No. 4, 2011. https://doi.org/10.1115/1.4003646.

[9] Weber, R., and Kühhorn, A., "Mistuning Identification Approach With Focus on High-Speed Centrifugal Compressors," *Journal of Engineering for Gas Turbines and Power*, Vol. 141, No. 3, 2018. https://doi.org/10.1115/1.4040999.

[10] Xu, K., Yan, X., Sun, W., and Wang, J., "Damping mistuning identification of coated blisks by means of vibrational test," *Journal of Sound and Vibration*, Vol. 463, 2019, p. 114954. https://doi.org/10.1016/j.jsv.2019.114954.

[11] Beirow, B., Kühhorn, A., Figaschewsky, F., Hönisch, P., Giersch, T., and Schrape, S., "Model update and validation of a mistuned high-pressure compressor blisk," *The Aeronautical Journal*, Vol. 123, No. 1260, 2019, pp. 230–247. https://doi.org/10.1017/aer.2018.149.

[12] Beirow, B., Kühhorn, A., and Nipkau, J., "An Equivalent Blisk Model Considering the Influence of the Air Flow on Blade Vibrations of a Mistuned Compressor Blisk," *Vibration Problems ICOVP 2011: The 10th International Conference on Vibration Problems*, Springer Netherlands, Dordrecht, 2011, pp. 549–555. https://doi.org/10.1007/978-94-007-2069-574.

[13] Beirow, B., Giersch, T., Kühhorn, A., and Nipkau, J., "Optimization-Aided Forced Response Analysis of a Mistuned Compressor Blisk," *Journal of Engineering for Gas Turbines and Power*, Vol. 137, No. 1, 2014. https://doi.org/10.1115/1.4028095.

[14] Lupini, A., Shim, J., Callan, S., and Epureanu, B. I., "Mistuning Identification Technique Based on Blisk Detuning," *AIAA Journal*, Vol. 59, No. 9, 2021, pp. 3087–3095. https://doi.org/10.2514/1.J060209.

Review copy- Do not distribute

[15] Cimpuieru, M., Kelly, S. T., Lupini, A., Keener, C., D'Souza, K., and Epureanu, B. I., "Mistuning Identification of Blisks Using Mass Detuning and Influence Coefficients," *AIAA Journal*, 2023. https://doi.org/10.2514/1.J062668.

[16] Zhou, B., Zhao, J., and Berruti, T. M., "Exploration of blade detuning tests for mistuning identification of blisks," *Mechanical Systems and Signal Processing*, Vol. 175, 2022, p. 109118. https://doi.org/10.1016/j.ymssp.2022.109118.

[17] Li, J., Aye-Addo, N., Kielb, R., and Key, N., "Mistuned Higher-Order Mode Forced Response of an Embedded Compressor Rotor—Part II: Mistuned Forced Response Prediction," *Journal of Turbomachinery*, Vol. 140, 2018, p. 031006. https://doi.org/10.1115/1.4038519.

[18] Gillaugh, D. L., Kaszynski, A. A., Brown, J. M., Beck, J. A., and Slater, J. C., "Mistuning Evaluation Comparison Via As-Manufactured Models, Traveling Wave Excitation, and Compressor Rigs," *Journal of Engineering for Gas Turbines and Power*, Vol. 141, No. 6, 2019. https://doi.org/10.1115/1.4042079.

[19] Gillaugh, D. L., Janczewski, T. J., Kaszynski, A. A., Brown, J. M., Beck, J. A., and Nessler, C., "Forced Response Variation of a Compressor Utilizing Blade Tip Timing, Strain Gages, and As-Manufactured Finite Element Models," *Journal of Engineering for Gas Turbines and Power*, Vol. 143, No. 11, 2021. https://doi.org/10.1115/1.4051358.

[20] Zhao, X., Li, H., Yang, S., Fan, Z., Dong, J., and Cao, H., "Blade vibration measurement and numerical analysis of a mistuned industrial impeller in a single-stage centrifugal compressor," *Journal of Sound and Vibration*, Vol. 501, 2021, p. 116068. https://doi.org/10.1016/j.jsv.2019.114954.

[21] Avalos, J., and Mignolet, M. P., "On Damping Entire Bladed Disks Through Dampers on Only a Few Blades," *Journal of Engineering for Gas Turbines and Power*, Vol. 132, No. 9, 2010, pp. 092503–10. https://doi.org/10.1115/1.3078792.

[22] Berruti, T., Firrone, C. M., and Gola, M. M., "A Test Rig for Noncontact Traveling Wave Excitation of a Bladed Disk With Underplatform Dampers," *Journal of Engineering for Gas Turbines and Power*, Vol. 133, No. 3, 2010. https://doi.org/10.1115/1.4002100.

[23] Firrone, C. M., and Berruti, T., "An Electromagnetic System for the Non-Contact Excitation of Bladed Disks," *Experimental Mechanics*, Vol. 52, No. 5, 2012, pp. 447–459. https://doi.org/10.1007/s11340-011-9504-1.

For Peer Review